repositorio institucional IMDEA Nanociencia

Fluorescence Modulation through the Inverted Energy Gap Law in Triply N−B←N-Containing Windmill-Shaped Triazines

Y. Feng, L. Wang, H. Gao, J. Zhou, M. Stolte, H. Qiu, L. Liu, V. Adebayo, M. Boggio-Pasqua, F. Würthner, J. Gierschner, Z. Xie

This is the peer reviewed version of the following article: Y. Feng, L. Wang, H. Gao, J. Zhou, M. Stolte, H. Qiu, L. Liu, V. Adebayo, M. Boggio-Pasqua, F. Würthner, J. Gierschner, Z. Xie, Angew. Chem. Int. Ed. 2025, 64, e202416425. https://doi.org/10.1002/anie.202416425 , which has been published in final form at https://onlinelibrary.wiley.com/doi/10.1002/anie.202416425

How to cite this version

Y. Feng, L. Wang, H. Gao, J. Zhou, M. Stolte, H. Qiu, L. Liu, V. Adebayo, M. Boggio-Pasqua, F. Würthner, J. Gierschner, Z. Xie. Fluorescence Modulation through the Inverted Energy Gap Law in Triply N−B←N-Containing Windmill-Shaped Triazines (2024), https://hdl.handle.net/20.500.12614/3836

Licence

This article may be used for non-commercial purposes in accordance with the Wiley Self-Archiving Policy https://olabout.wiley.com/WileyCDA/Section/id820227.html (last accessed November 2025)

Embargo

This version (post-print or accepted manuscript) of the article has been deposited in the Institutional Repository of IMDEA Nanociencia with access rights embargoed until 31.10.2025.

Fluorescence Modulation through the Inverted Energy Gap Law in Triply N—B←N-Containing Windmill-Shaped Triazines

Yi Feng[a], Liangxuan Wang[b,c], Hongcheng Gao[a], Jiadong Zhou[a], Matthias Stolte[d], David Bialas[d], Honglin Qiu[a], Linlin Liu[a], Victor Adebayo[e], Martial Boggio-Pasqua[e], Frank Würthner[d], Johannes Gierschner*[b], and Zengqi Xie*[a]

[a] Institute of Polymer Optoelectronic Materials and Devices, State Key Laboratory of Luminescent Materials and Devices, South China University of Technology (SCUT), 510640 Guangzhou (P. R. China).

[b] Madrid Institute for Advanced Studies, IMDEA in Nanoscience, C/ Faraday 9, Ciudad Universitaria Cantoblanco, 28049 Madrid (Spain).

[c] Institute of Physical and Theoretical Chemistry, Eberhard Karls University Tübingen, Auf der Morgenstelle 18, 72076 Tübingen (Germany).

[d] Institut für Organische Chemie & Center for Nanosystems Chemistry, Universität Würzburg, Am Hubland, 97074 Würzburg (Germany).

[e] Laboratoire de Chimie et Physique Quantiques, FeRMI, Université Toulouse III-Paul Sabatier, CNRS, 31062 Toulouse (France).

Supporting Information Placeholder

ABSTRACT: A series of windmill-shape heterocyclic molecules containing three N—B←N units, TBN and its derivatives, containing quasi-planar C_3 symmetric backbone, are synthesized through a threefold reaction of trisubstituted triazine and triphenylborane. TBN shows a strongly allowed, two-fold degenerate lowest excited state, but suffers from very low fluorescence, due to efficient nonradiative decay through a conical intersection (CI) as revealed by femtosecond transient absorption spectroscopy and quantum-chemical calculations. Introducing peripheral phenyl- and thienyl-groups in the molecular structure (Ph-TBN and Th-TBN), pronounced bathochromic shifts are observed. The nonradiative pathway is inhibited by the increased energy barriers to access the CI. As a result, these compounds are highly fluorescent. The strategy towards compounds which follow such 'inverted energy gap law' might be of interest to design novel emissive materials.

Extended heterocyclic π-conjugated molecules have gained great attentions for the distinguished optoelectronic properties and promising applications in organic electronic devices.[1-7] Heteroatoms, especially boron (B) and nitrogen (N) as neighbor elements to carbon (C), are particularly utilized to replace carbon atoms, which not only greatly increases the diversity of organic materials but may also significantly improve the optoelectronic functionality.[8-11] For instance, highly efficient narrowband emission was recently achieved in a BN-containing polycyclic molecule to reduce vibronic coupling in the emission process.[12] Fast intersystem crossing (ISC) as well as efficient thermally activated delayed fluorescence (TADF) were reported in BN-containing heteroaromatics,[13,14] due to small exchange energies as induced by an uncommon short-range charge-transfer (CT) character of the emitting state.[15] In particular, B←N is isoelectronic to C═C, but reveals a dipolar nature due to the coordination bond, and thus offers opportunities to tune the molecular energy levels by the insertion of B←N units, e.g. to meet the specific demands in organic solar cells (OSCs) as electron acceptors.[16,17] As a typical chromophore, boron dipyrromethene (BODIPY), bearing N—B←N unit in molecular structure, is usually highly fluorescent and thereby suitable for chemical sensors.[18-20] During the past years, a multitude of novel N—B←N containing chromophores were reported as fluorescent materials in organic light-emitting diodes (OLEDs).[21,22]

The synthesis of planar BN-containing π-scaffolds is of particular interest because of extended conjugation, introduction of multiple functional groups and favored π-packing morphologies.[23,24] Bonifazi et al reported BN-containing coronene derivatives with enhanced fluorescence compared to the all-carbon isoelectric molecule.[25] Previous studies by Pei et al indicated that BN-containing heterosuperbenzene exhibit good charge transport properties for the assembled π-stacks.[26] Star-shaped BN-containing planar π-scaffolds, especially in C_3 symmetry, however, were seldom discussed, possibly due to lack of fluorescence. One of the few examples was reported by Zhang et al, being trinaphthylene analogues with triple N—B←N units; the very low fluorescence yield of these molecules was attributed to efficient nonradiative deactivation, arising from the floppy molecular structure.[27,28] Finally, the synthesis of BN-containing aromatics is usually conditionally harsh and time-consuming, and it still remains as a great challenge to introduce multiple boron and nitrogen atoms into a π-system.[29,30] Facile synthetic methods to construct stable and multi-BN-containing π-scaffolds is of essential importance for the creation of new functional materials, eventually with improved fluorescence properties.

Herein, we provide a convenient synthetic route to windmill-shaped molecules,[31] termed as TBN, which contains three N—B←N units in a C_3 symmetric π-scaffold (Figure 1a). The core

unit possesses a nearly planar backbone structure and can be easily derived by introducing various substituents on the peripheral positions. The parent TBN molecule shows low fluorescence in dilute solution and solid state, but its derivatives with rotatable peripheral phenyl and thienyl substituents (Ph-TBN and Th-TBN) turned out to be highly fluorescent. Steady-state and time-resolved absorption and fluorescence experiments, combined with quantum-chemical calculations based on time-dependent density functional theory (TD-DFT) and its mixed-reference spin-flip (MR-SF-TD-DFT) variant, indicate that the exited state of TBN undergoes efficient nonradiative decay through a conical intersection (CI). Conversely, this nonradiative pathway is less accessible for Ph-TBN and Th-TBN due to an increased excited-state energy barrier to reach the CI region, establishing a rare example for the 'inverted energy gap law'.[32]

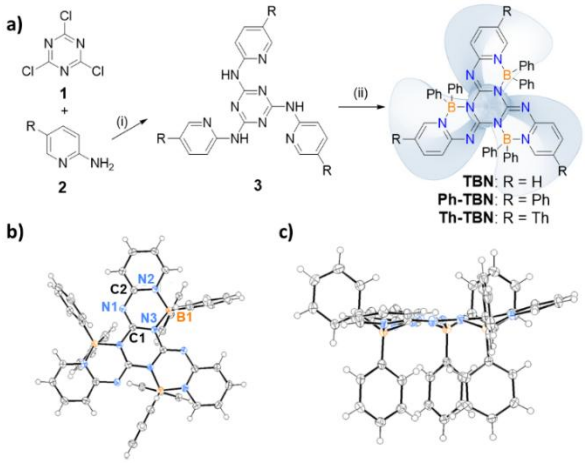

Figure 1. a) Synthetic route of windmill-shaped TBN and its derivatives. (i) Triethylamine, toluene, 110 °C, 12 h; (ii) toluene, 110 °C, 48 h. b) Top view of TBN in the crystal. The bond lengths are 1.302 Å for C1-N1, 1.359 Å for C2-N1, 1.602 Å for B1-N2 and 1.615 Å for B1-N3. c) Side view of TBN. The boron atoms are off plane giving asymmetric distribution of the phenyl substituents relative to the backbone.

The synthetic route towards TBN and its derivatives, Ph-TBN and Th-TBN, is illustrated in Figure 1a. Firstly, the intermediate compounds (**3**) were synthesized through a threefold reaction between cyanuric chloride and 2-aminopyridine; then, the crude products (brown solid) were used directly to react with triphenylborane to get the final target compounds. The chemical structures of the final products were well evidenced by ^{1}H and ^{13}C NMR spectra (Figures S1-S6), HRMS (where are the data?), as well as single crystal X-ray analysis (Table S1-S2, Figures S7-S8). Although the total yields are not high (~15%), all the reactants and reagents are readily available, and also the reaction conditions are mild. Thus, the advocated synthetic route to such windmill-shaped molecules with extended conjugated heterocycles is highly efficient and time-saving. All the three target compounds are well soluble in common solvents, like chloroform, toluene etc., mainly owning to the six flexible phenyl rings attached at the three boron atoms. Although three N—B←N units are contained in the TBN compounds, the thermal stability is excellent with decomposition temperatures all above 380 °C, tested by thermogravimetric analysis (Figure S9).

Single crystals of the three target compounds were grown by recrystallization from CH_2Cl_2/C_2H_5OH/toluene solutions, and the crystal data are depicted in Table S1. As shown in Figure 1 and Figure S7, the heterocyclic core of TBN exhibits a large and approximately planar π-scaffold with a spatial C_3 symmetry. Owing to the weak van der Waals' forces in the crystal lattice, the six phenyl groups linked to the boron atoms exhibit asymmetric distribution relative to the backbone plane, resulting in a slight skeletal distortion (Figure 1c). In Ph-TBN, the peripheral phenyl groups show the torsion angles of 25.2°, 28.7° and 32.8° relative to the central scaffold; for Th-TBN, one of the peripheral thienyl group shows positional disorder in the X-ray structure, and the torsion angles between the thienyl groups and the central scaffold are largely different, i.e. 1.8°, 11.6° and 25.5°, respectively; this, however, can be ascribed to packing effects, as the DFT geometry optimizations indicate C_3 symmetry as in TBN.

The B-N linkage in TBN is worth being explored for its unique character of chemical bonding. For some six-member rings containing the N—B←N unit, usually one shorter covalent bond (of about 1.49 Å) and one longer coordination bond (about 1.58 Å) are found.[33] However, in TBN, the average bond length from boron to nitrogen (B1-N3) is 1.615 Å, which is almost equal to that of B1-N2 at 1.602 Å (Table S2). The DFT results indeed confirm these results (1.61 Å; Table S4). Therefore, the BN bonding situation in the TBN family is rather comparable to that of Ph-substituted BODIPY.[34,35] Significantly, the average bond length of C1-N1 is 1.302 Å, which is much shorter than that of C2-N1 bond (1.359 Å), indicating double bonding for C1-N1 and single bonding for C2-N1 as a favored Kekulé structure, which is confirmed by the DFT results (Table S4). Hence, the chemical structure of TBN shown in Figure 1a indeed represents the bonding situation found experimentally, although several resonance structures are possible (Figure S10). Considering that the N2 in the pyridine ring and N3 in the triazine ring are both electron-deficient, it seems impossible to react with boron by covalent bonding.

The absorption and fluorescence spectra of the TBN series are displayed in Figure 2 and the corresponding spectral and photophysical data are listed in Table 1. All compounds show vibronically-structured absorption bands in the violet/blue region with molar

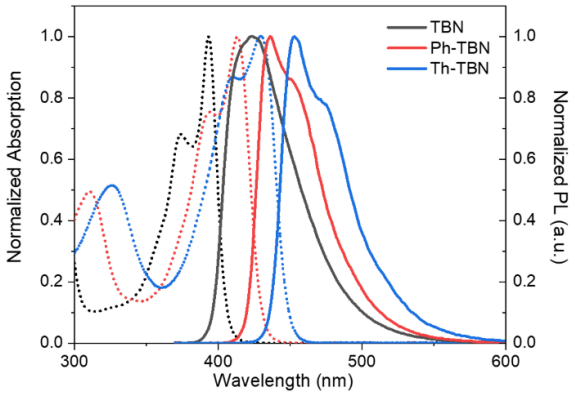

Figure 2. Normalized absorption spectra (dotted line) and fluorescence spectra (solid line), measured in 10^{-5} M toluene solution at room temperature.

Table 1. Spectral data of the compounds, measured in toluene (10^{-5} M): absorption and fluorescence maxima ($\lambda_{abs,F}$), maximum molar extinction coefficients (ε_m), fluorescence quantum yields and lifetimes (Φ_F, τ_F), radiative and non-radiative rates obtained as $k_F = \Phi_F/\tau_F$ and $k_{nr} = (1-\Phi_F)/\tau_F$.

Molecule	λ_{abs} / ε_m (nm / 10^4 $M^{-1}cm^{-1}$)	λ_F (nm)	Φ_F [a]	τ_F (ns)	k_F (ns^{-1})	k_{nr} (ns^{-1})
TBN	393 / 8.32	424	~0.01	0.08 [b]	~0.12	~12
Ph-TBN	413 / 9.27	436	0.35	1.29 [c]	0.27	0.51
Th-TBN	430 / 9.37	453	0.47	1.59 [c]	0.30	0.33

[a] From absolute measurements in an integrating sphere (see SI for details). [b] From fs-TA experiments (see text and SI for details). [c] From TCSPC measurements (see SI for details).

extinction coefficients (ε_m) of about 8 to 9 × 10^4 M^{-1} cm^{-1}, see Table 1. According to our TD-DFT calculations (M06-2X/6-31G(d); see computational details in SI), the high ε_m values result from a two-fold degenerate electronic transition to the first and second excited state ($S_0 \rightarrow S_{1,2}$) with pronounced locally-excited (LE) character residing on the molecular core structure, see Figure 3. The LE character is further confirmed by the weak dependence of the optical spectra on solvent polarity (Figure S11). Introduction of the Ph- and Th-moieties in the TBN backbone leads to a pronounced bathochromic shift of absorption, i.e. from 393 nm to 413 and 430 nm, respectively, due to the extension of the frontier molecular orbitals towards the Ph and Th groups (Figure 3). This redshift is reproduced by the TD-DFT calculations (Table 2), while the transition energies are clearly overestimated by the M06-2X functional.[36] Similar vibronic features are observed for the absorption spectra of the three compounds. This result suggests similar vibrational relaxation from the Franck-Condon (FC) region to the local S_1 minimum structure. In addition, the S_1 vibrational relaxation is associated with relaxation energies (ΔE^{rel}, Table 2) of 0.18 eV for TBN and of 0.26 eV for Ph- and Th-TBN. The larger ΔE^{rel} values in Ph- and Th-TBN are probably related to the fact that the S_0 structures are quasi-planar for these two compounds, whereas it is not in TBN (Figure S15).

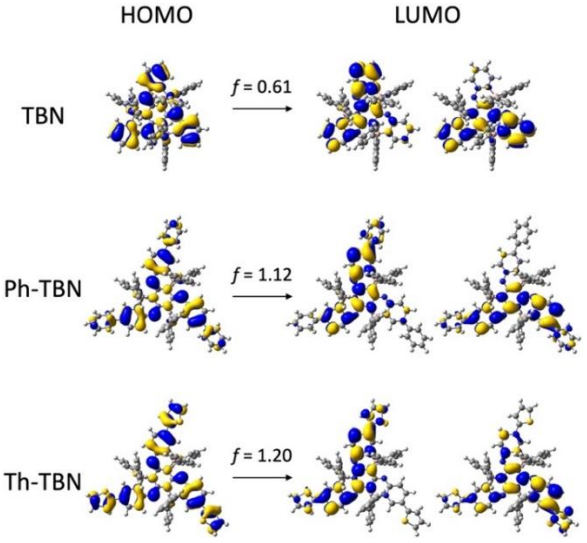

Figure 3. Frontiers molecular orbitals of TBN, Ph-TBN and Th-TBN. The S_1 and S_2 electronic states are degenerate at the C_3 symmetric ground-state geometry, as they involve electronic transitions from the HOMO to the pair of degenerate LUMOs. *f* is the oscillator strength for the corresponding vertical transition.

In agreement with the absorption data, the fluorescence spectra show a gradual redshift from TBN to Ph- and Th-TBN with peak maxima at 424, 436 and 453 nm, respectively (Figure 2). This redshift is well reproduced by the theoretical calculations when one considers the 0–0 transitions (Table 2). However, while the PL spectra of Ph-TBN and Th-TBN are vibronically structured, the fluorescence spectrum of the parent TBN compound is broad and unstructured. The approximate mirror symmetry between absorption and fluorescence usually indicates similar equilibrium geometries on the ground and first excited states (S_0, S_1) potential energy surfaces (PES), from where absorption and emission, respectively, emerge.[37] In this scenario, fluorescence occurs from the minimum on the S_1 PES, close to the initially populated FC point. This is obviously the case for Ph- and Th-TBN. However, the breakdown of the mirror symmetry and structureless emission band in TBN point to potentially larger geometrical reorganizations on the S_1 PES,[38,39] and access to conical intersections. This observation is confirmed by our theoretical calculations (vide infra).

This pronounced difference between the Ph- and Th-TBN on one side and the parent TBN compound on the other is directly reflected in largely different excited state deactivation kinetics. Indeed, while Ph- and Th-TBN are highly emissive in dilute solution with fluorescence quantum yield Φ_F as high as 35% and 47%, respectively, TBN is little fluorescent with Φ_F of about 1% (Table 1). The associated fluorescence lifetime τ_F of TBN is below the resolution of our time-correlated single photon counting (TCSPC) setup (ca. 100 ps); therefore, τ_F was determined by transient absorption (TA; *vide infra*) to 0.08 ns. In stark contrast, τ_F of Ph- and Th-TBN are 1.29 and 1.59 ns (see Table 1). From this, the radiative rate can be calculated as $k_F = \Phi_F / \tau_F$, which are of the same order for all three compounds (Table 1), in agreement with the TD-DFT results which indeed predict a symmetry-allowed S_1 state for all compounds (Figure S16).[40] Therefore, the large difference in the deactivation kinetics can be directly traced back to a strongly enhanced nonradiative decay rate k_{nr} in TBN, which is two orders of magnitude larger compared to the Ph- and Th-substituted species, see Table 1. At a first glance, this behavior may appear counterintuitive, as the FC energy of TBN (reflected in the absorption maxima) is the highest among the compounds; therefore, from the 'energy gap law' (EGL), which is derived from a simple Fermi's golden rule picture,[41] one would expect the lowest k_{nr} for TBN. The present results thus evidence an 'inverted EGL'. This was indeed established earlier for other compound families[32,42,43] and was traced back to the ultrafast deactivation kinetics through a conical intersection (CI).[44]

Table 2. Theoretical values for energetics (in eV) relevant to the photophysical behavior of TBN compounds in toluene.[a]

Molecule	TBN	Ph-TBN	Th-TBN
ΔE^{va} / eV	3.73	3.58	3.47
λ^{va} / nm	332	346	357
f^{va}	0.61	1.12	1.20
ΔE^{ve} / eV	2.96	2.97	2.93

λ^{ve} / nm	419	417	423
f^{ve}	0.28	0.62	0.83
ΔE_{00} / eV	3.45	3.22	3.11
ΔE^{rel} / eV	0.18	0.26	0.26
(kcal/mol)	(4.1)	(5.9)	(5.9)
$\Delta E^{\ddagger}$ / eV	0.21	0.28	0.32
(kcal/mol)	(4.9)	(6.5)	(7.5)
ΔE^{cyc} / eV	-0.24	-0.17	-0.10
(kcal/mol)	(-5.6)	(-3.9)	(-2.4)
ΔE^{CI} / eV	-0.23	-0.16	-0.10
(kcal/mol)	(-5.3)	(-3.7)	(-2.4)

[a] Vertical absorption (ΔE^{va}), vertical emission (ΔE^{ve}), 0–0 transition (ΔE_{00}), S_1 relaxation energy (ΔE^{rel}), S_1 energy barrier ($\Delta E^{\ddagger}$), S_1 cyclization energy (ΔE^{cyc}) were computed with TD-DFT/6-31G(d) in toluene; S_1 energy to conical intersection (ΔE^{CI}) was obtained from MR-SF-TD-DFT calculations. See Fig. 5 for graphical description of the energy parameters. *f*: oscillator strengths for vertical absorption (f^{va}) and emission (f^{ve}).

To investigate the ultrafast deactivation kinetics, femtosecond transient absorption (fs-TA) spectra were recorded for TBN in benzonitrile. The fs-TA map in Figure 4 exhibits a ground state bleaching (GSB) at 360-400 nm (negative TA), a weak stimulated emission (SE) signal at 400-450 nm (positive TA), as well as an excited state absorption (ESA) at > 450 nm. Global analysis procedure allowed to extract two time constants with $\tau_1 \approx 9$ ps and $\tau_2 \approx 84$ ps. The shorter time constant is very similar to that observed for Ph- and Th-TBN (Figure S12), and is thus assigned to the initial structural relaxation in S_1.[45] The longer component τ_2 in TBN is associated with the path towards the CI; the considerable structural changes are directly seen in the spectral change of the SE signal. The latter develops from an initial state with sharp spectral features, which mirror the GSB, towards a structureless spectrum, which resembles the steady-state fluorescence (Figure 2). Conversely, Ph- and Th-TBN miss τ_2 but instead display a lifetime in the TA experiment (Figure S12), which corresponds to the fluorescence lifetime τ_F found in the TCSPC experiment (Table 1). Finally, Ph- and Th-TBN exhibit another long component of hundreds of nanoseconds (Figure S12), which can be assigned to the population of the triplet manifold through inter-system crossing (ISC).

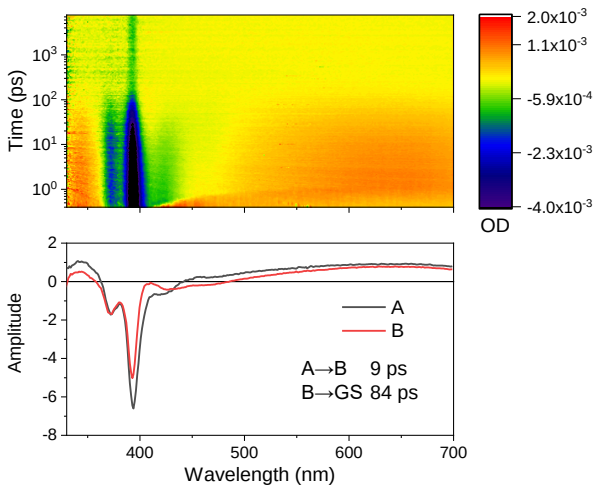

Figure 4. The fs-TA spectra of TBN in benzonitrile (top) and the evolution-associated spectra (EAS) A→B (IC process) and B→GS (recombination), respectively (bottom).

To rationalize the difference of photophysical behavior between the Ph- and Th-TBN compounds on one side and the parent TBN compound on the other side, we investigated computationally the topography of the S_0 and S_1 PES for each system at the TD-DFT and MR-SF-TD-DFT levels (see computational details in SI) along the main non-radiative deactivation pathway leading to the CI. The potential energy profiles are schematized in Figure 5 along with the main relevant parameters considered for discussion. In particular, the excited-state barrier computed at the TD-DFT level and the location of the conical intersection at the MR-SF-TD-DFT level are of critical importance. The values of these parameters are reported in Table 2 for each compound.

For all three compounds, a local S_1 minimum responsible for the fluorescence has been identified (Figure S15). It corresponds to an excited-state structure displaying significant out-of-plane deformations and a substantial shortening (–0.4 Å) of the C—N distance between a C_α of a phenyl ring attached to a B atom of one N—B←N unit to the closest N center of a nearby N—B←N unit. In addition, its electronic structure starts developing CT character between the three N—B←N arms (Figure S16). A striking result is the presence of a second local S_1 minimum displaying a cyclized structure (denoted S_1 cyclized minimum in Fig. 5). The cyclization takes place between the aforementioned C_α of a phenyl ring to the closest N center of a nearby N—B←N unit, as illustrated in Figure 5. To populate this transient cyclized structure, an excited-state barrier has to be overcome, being ($\Delta E^{\ddagger}$) of 0.21 eV (4.9 kcal/mol), 0.28 eV (6.5 kcal/mol), 0.32 eV (7.5 kcal/mol) for TBN, Ph-TBN and Th-TBN, respectively (Table 2, Figure S17). Taking into account thermal and entropic contributions at room temperature, the activation Gibbs free energies are 5.4, 8.7 and 10.9 kcal/mol, respectively. The S_1 cyclization energies (ΔE^{cyc}) are all negative indicating that the S_1 cyclized minima lie energetically below the S_1 local minima. In particular, we stress that ΔE^{cyc} is significantly more negative (–5.6 kcal/mol) in TBN compared to Ph-TBN (–3.9 kcal/mol) and Th-TBN (–2.4 kcal/mol). The corresponding Gibbs free energies are –0.9, 1.6 and 5.6 kcal/mol, respectively. Combined with the information on the S_1 cyclization barriers, these results unambiguously point to a more favorable photocyclization in TBN compared to Ph- and Th-TBN, both from the energetic and kinetic aspects. Importantly, these cyclized structures are associated with more pronounced CT character and small S_0–S_1 energy gaps (Figure S18). We note that the S_0/S_1 CI are all located in the vicinity of the cyclized minimum structures (see Figure 5), where the energy difference between the S_1 cyclized minimum and the CI are less than 0.3 kcal/mol. This implies that once the system undergoes the photocyclization in the S_1 excited state, very efficient non-radiative decay will take place to the S_0 state leading to reformation of the original ground-state molecule (no cyclized structure could be identified on the S_0 PES). The S_0/S_1 cyclized CI thus provide an efficient decay pathway for photostability.

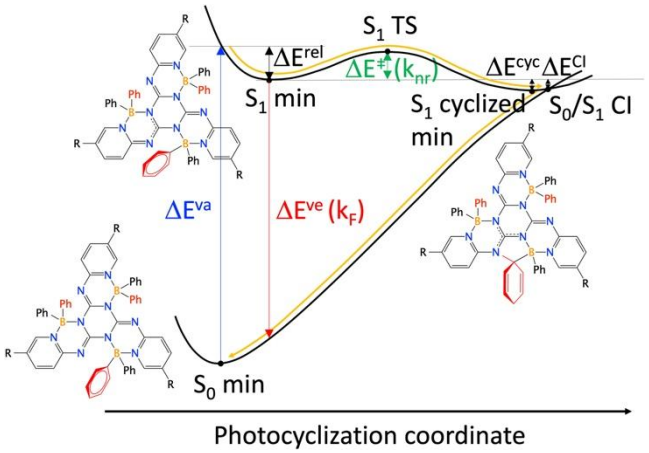

Figure 5. Schematic potential energy profile for the TBN series of compounds showing a radiationless photophysical pathway (yellow line) controlled by an activated photocyclization mechanism followed by ground-state recovery after decay at a cyclized conical intersection.

These theoretical results can be put into perspective with the experimental observations. In all three compounds, the 9 ps time constant corresponds to initial excited-state relaxation to the first local S_1 minimum (S_1 min; Fig. 5) responsible for fluorescence. In TBN only, the CI can be thermally reached within 84 ps, a timescale much shorter than that required for radiative deactivation via the local S_1 minimum. This can be monitored by low temperature (LT) fluorescence spectroscopy (Figure S13a, Table S3), which recovers the structured emission as observed for Ph- and Th-TBN. Concomitantly, the fluorescence intensity of TBN increases significantly at LT. On the other hand, experiments in rigid environments (i.e. in a PMMA matrix, and as powder) at room temperature (RT) hardly increase the fluorescence (see Figure S14). This clearly evidences that the structural deformation to reach the CI does not require very extensive geometrical reorganization by large amplitude motions as observed in floppy systems.[39,44,46] This is consistent with our calculations showing a compact cyclized structure for the CI, where its access is solely controlled by temperature, but not by viscosity. Therefore, TBN is dark at RT both in solution as well as a molecular solid (powder). Thus, no solid-state luminescence enhancement (SLE) [39,47] is observed, as it is commonly found for floppy compounds.[46,47]

For Ph- and Th-TBN, the access to the CI is more difficult, with a substantially increased potential energy barrier and a less favorable excited-state cyclization energy. As a consequence, the non-radiative deactivation channel through photocyclization is inhibited in Ph- and Th-TBN, which deactivate effectively by the radiative channel from the local S_1 minimum. This mechanistic picture provides a rationale for the experimentally observed inverted EGL.

In conclusion, a series of windmill-shape heterocyclic BN-based triazines were designed and synthesized. TBN, containing three N—B←N units, was rather easily obtained by a two-step route with a series of threefold reactions. Concomitantly, Ph-TBN and Th-TBN were obtained with peripheral substitution. The crystal structures show that the heteroatoms and substituents slightly distort the central scaffold compared to the planar trinaphthalene, exhibiting C_3 symmetry. The B—N bonding situation in TBN was discussed based on the single crystal structures and DFT calculations. All TBN compounds show strong two-fold degenerate $S_0 \rightarrow S_{1,2}$ transitions but the excited-state deactivation differs largely. While Ph- and Th-TBN are highly fluorescent, the emission of TBN is effectively quenched, although the FC energy is the highest among the compounds. This 'inverted energy gap law' behavior[32] is rationalized by the different temperature-controlled access to the rigid-core cyclized conical intersection (CI), as revealed by MR-SF-TD-DFT calculations. This drives the nonradiative decay by internal conversion, as indeed monitored by ultrafast transient absorption spectroscopy.

ASSOCIATED CONTENT

Supporting Information

The Supporting Information is available free of charge on the ACS Publications website.

Materials and methods; synthesis and characterization; single-crystal data; resonance structures; spectra; calculated ground and excited state electronic features; cyclic-voltammetry (data not used and referenced anywhere?); thermo gravimetric analysis and differential scanning calorimetry (data not used and referenced anywhere?). (PDF)

Crystallographic information files for TBN, Ph-TBN and Th-TBN. (CIF)

XYZ files for cartesian coordinates of TBN, Ph-TBN and Th-TBN optimized structures. (ZIP)

AUTHOR INFORMATION

Corresponding Author

johannes.gierschner@imdea.org; msxiez@scut.edu.cn.

Notes

The authors declare no competing financial interests.

ACKNOWLEDGMENT

The work at SCUT was supported by the National Natural Science Foundation of China (21975076, 21733005, 52003089, 51521002), and at IMDEA was supported by the Spanish Ministry for Science (MINECO–FEDER project PID2022-138222NB-C21) by the 'Severo Ochoa' program for Centers of Excellence in Research and Development (MINECO grant SEV2016-0686) and the Campus of International Excellence UAM + CSIC. We also thank the support from SCUT within the 111 program. This work was granted access to the HPC resources of CALMIP supercomputing center under the allocation 2024-[12158].

REFERENCES AND NOTES

(1) Chatterjee, T.; Shetti, V. S.; Sharma, R.; Ravikanth, M. Heteroatom-containing porphyrin analogues. *Chem. Rev.* **2017**, *117*, 3254.

(2) McConnell, C. R.; Liu, S.-Y. Late-stage functionalization of BN-heterocycles. *Chem. Soc. Rev.* **2019**, *48*, 3436.

(3) Huang, Z.; Wang, S.; Dewhurst, R. D.; Ignat'ev, N. V.; Finze, M.; Braunschweig, H. Boron: its role in energy-related processes and applications. *Angew. Chem. Int. Ed.* **2020**, *59*, 8800.

(4) Wang, J. Y.; Zhan, X. W. Fused-ring electron acceptors for photovoltaics and beyond. *Acc. Chem. Res.* **2021**, *54*, 132.

(5) Lee, Y. H.; Jang, M.; Lee, M. Y.; Kweon, O. Y.; Oh, J. H. Flexible field-effect transistor-type sensors based on conjugated molecules. *Chem.* **2017,** *3*, 724.

(6) Ando, N.; Yamada, T.; Narita, H.; Oehlmann, N. N.; Wagner, M.; Yamaguchi, S. Boron-doped polycyclic π-electron systems with an antiaromatic borole substructure that forms photoresponsive B–P lewis adducts. *J. Am. Chem. Soc.* **2021**, *143*, 9944.

(7) Cloke, R. R.; Marangoni, T.; Nguyen, G. D.; Joshi, T.; Rizzo, D. J.; Bronner, C.; Cao, T.; Louie, S. G.; Crommie, M. F.; Fischer, F. R. Site-specific substitutional boron doping of semiconducting armchair graphene nanoribbons. *J. Am. Chem. Soc.* **2015**, *137*, 8872.

(8) Campbell, P. G.; Marwitz, A. J. V.; Liu, S.-Y. Recent advances in azaborine chemistry. *Angew. Chem. Int. Ed.* **2012**, *51*, 6074.

(9) Wang, X. Y.; Wang, J. Y.; Pei, J. BN heterosuperbenzenes: synthesis and properties. *Chem-Eur. J.* **2015**, *21*, 3528.

(10) Wakamiya, A.; Taniguchi, T.; Yamaguchi, S. Intramolecular B-N coordination as a scaffold for electron-transporting materials: synthesis and properties of boryl-substituted thienylthiazoles. *Angew. Chem. Int. Ed.* **2006,** *45*, 3170.

(11) Palomino-Ruiz, L.; Rodríguez-González, S.; Fallaque, J. G.; Márquez, I. R.; Agraït, N.; Díaz, C.; Leary, E.; Cuerva, J. M.; Campaña, A. G.; Martín, F.; Millán, A.; González, M. T. Single-molecule conductance of 1, 4-azaborine derivatives as models of BN-doped PAHs. *Angew. Chem. Int. Ed.* **2021**, *60*, 6609.

(12) Kondo, Y.; Yoshiura, K.; Kitera, S.; Nishi, H.; Oda, S.; Gotoh, H.; Sasada, Y.; Yanai, M.; Hatakeyama, T. Narrowband deep-blue organic light-emitting diode featuring an organoboron-based emitter. *Nat. Photonics* **2019,** *13*, 678.

(13) Ahn, D. H.; Kim, S. W.; Lee, H.; Ko, I. J.; Karthik, D.; Lee, J. Y.; Kwon, J. H. Highly efficient blue thermally activated delayed fluorescence emitters based on symmetrical and rigid oxygen-bridged boron acceptors. *Nat. Photonics* **2019,** *13*, 540.

(14) Suresh, S. M.; Duda, E.; Hall, D.; Yao, Z.; Bagnich, S.; Slawin, A. M. Z.; Baessler, H.; Beljonne, D.; Buck, M.; Olivier, Y.; Koehler, A.; Zysman-Colman, E. A deep blue B, N-doped heptacene emitter that shows both thermally activated delayed fluorescence and delayed fluorescence by triplet–triplet annihilation. *J. Am. Chem. Soc.* **2020,** *142*, 6588.

(15) Pershin, A.; Hall, D.; Lemaur, V.; Sancho-Garcia, J.-C.; Muccioli, L.; Zysman-Colman, E.; Beljonne, D.; Olivier, Y. Highly emissive excitons with reduced exchange energy in thermally activated delayed fluorescent molecules. *Nat. Commun.* **2019,** *10*, 597.

(16) Dou, C.; Ding, Z.; Zhang, Z.; Xie, Z.; Liu, J.; Wang, L. Developing conjugated polymers with high electron affinity by replacing a C=C unit with a B←N unit. *Angew. Chem. Int. Ed.* **2015,** *54*, 3648.

(17) Zhao, R.; Liu, J.; Wang, L. Polymer acceptors containing B←N units for organic photovoltaics. *Acc. Chem. Res.* **2020,** *53*, 1557.

(18) Loudet, A.; Burgess, K. BODIPY dyes and their derivatives: syntheses and spectroscopic properties. *Chem. Rev.* **2007,** *107*, 4891.

(19) Ulrich, G.; Ziessel, R.; Harriman, A. The chemistry of fluorescent bodipy dyes: versatility unsurpassed. *Angew. Chem. Int. Ed.* **2008,** *47*, 1184.

(20) Patalag, L. J.; Hoche, J.; Holzapfel, M.; Schmiedel, A.; Mitric, R.; Lambert, C.; Werz, D. B. Ultrafast resonance energy transfer in ethylene-bridged BODIPY heterooligomers: from frenkel to förster coupling limit. *J. Am. Chem. Soc.* **2021**, *143*, 7414.

(21) Mas-Montoya, M.; Montenegro, M. F.; Espinosa Ferao, A.; Tarraga, A.; Neptuno Rodriguez-Lopez, J.; Curiel, D. Rigid π-extended boron difluoride complex with mega-stokes shift for bioimaging. *Org. Lett.* **2020,** *22*, 3356.

(22) Li, D.; Zhang, H.; Wang, Y. Four-coordinate organoboron compounds for organic light-emitting diodes (OLEDs). *Chem. Soc. Rev.* **2013,** *42*, 8416.

(23) Zhu, C.; Ji, X.; You, D.; Chen, T. L.; Mu, A. U.; Barker, K. P.; Klivansky, L. M.; Liu, Y.; Fang, L. Extraordinary redox activities in ladder-type conjugated molecules enabled by B←N coordination-promoted delocalization and hyperconjugation. *J. Am. Chem. Soc.* **2018,** *140*, 18173.

(24) Min, Y.; Dou, C.; Liu, D.; Dong, H.; Liu, J. Quadruply B← N-fused dibenzo-azaacene with high electron affinity and high electron mobility. *J. Am. Chem. Soc.* **2019,** *141*, 17015.

(25) Dosso, J.; Tasseroul, J.; Fasano, F.; Marinelli, D.; Biot, N.; Fermi, A.; Bonifazi, D. Synthesis and optoelectronic properties of hexa-perihexabenzoborazinocoronene. *Angew. Chem. Int. Ed.* **2017,** *56*, 4483.

(26) Wang, X.-Y.; Zhuang, F.-D.; Wang, R.-B.; Wang, X.-C.; Cao, X.-Y.; Wang, J.-Y.; Pei, J. A straightforward strategy toward large BN-embedded π-systems: Synthesis, structure, and optoelectronic properties of extended BN heterosuperbenzenes. *J. Am. Chem. Soc.* **2014,** *136*, 3764.

(27) The very small PLQY with the long PL lifetime implies a small radiative rate, which apparently cannot compete with the nonradiative rate.

(28) Qiu, F.; Zhang, F.; Tang, R.; Fu, Y.; Wang, X.; Han, S.; Zhuang, X.; Feng, X. Triple boron-cored chromophores bearing discotic 5,11,17-triazatrinaphthylene-based ligands. *Org. Lett.* **2016,** *18*, 1398.

(29) Fingerle, M.; Dingerkus, J.; Schubert, H.; Wurst, K. M.; Scheele, M.; Bettinger, H. F. Heteroatom cycloaddition at the $(BN)_2$ bay region of dibenzoperylene. *Angew. Chem. Int. Ed.* **2021,** *60*, 15798.

(30) Scholz, A. S.; Massoth, J. G.; Bursch, M.; Mewes, J.-M.; Hetzke, T.; Wolf, B.; Bolte, M.; Lerner, H.-W.; Grimme, S.; Wagner, M. BNB-doped phenalenyls: modular synthesis, optoelectronic properties, and one-electron reduction. *J. Am. Chem. Soc.* **2020**, *142*, 11072.

(31) We prefer the term 'windmill-shaped' against the more general term 'star-shaped' for the precision of the former. For an in-depth review on star-shaped π-conjugated systems, see Kanibolotsky, A. L.; Perepichka, I. F.; Skabara, P. J. Star-shaped π-conjugated oligomers and their applications in organic electronics and photonics. *Chem. Soc. Rev.* **2010,** *39*, 2695.

(32) Shi, J.; Izquierdo, M. A.; Oh, S.; Park, S. Y.; Milián-Medina, B.; Roca-Sanjuán, D.; Gierschner, J. Inverted energy gap law for the nonradiative decay in fluorescent floppy molecules: larger fluorescence quantum yields for smaller energy gaps. *Org. Chem. Front.* **2019,** *6*, 1948.

(33) Dou, C.; Long, X.; Ding, Z.; Xie, Z.; Liu, J.; Wang, L. An electron-deficient building block based on the B←N unit: an electron acceptor for all-polymer solar cells. *Angew. Chem. Int. Ed.* **2016,** *55*, 1436.

(34) Wang, M.; Vicente, M. G. H.; Mason, D.; Bobadova-Parvanova, P. Stability of a series of BODIPYs in acidic conditions: an experimental and computational study into the role of the substituents at boron. *ACS Omega* **2018,** *3*, 5502.

(35) Yang, L.; Drew, B.; Yalagala, R. S.; Chaviwala, R.; Simionescu, R.; Lough, A. J.; Yan, H. Crystal structure and solvent-dependent behaviours of 3-amino-1, 6-diethyl-2, 5, 7-trimethyl-4, 4-diphenyl-3a, 4a-diaza-4-bora-s-indacene. *Acta Crystallogr. E* **2017,** *73*, 378.

(36) The use of the standard B3LYP functional gives a much better agreement between the computed vertical transition energies and the experimental absorption maxima. However, this is only true for transitions occurring near the FC region because of the LE character of the S_1 and S_2 states in that region. Upon excited-state geometry relaxation, S_1 gains substantial CT character (Figures S15-S17) and B3LYP becomes unreliable.

(37) Gierschner, J.; Mack, H.-G.; Lüer, L.; Oelkrug, D. Fluorescence and absorption spectra of oligophenylenevinylenes: Vibronic coupling, band shapes, and solvatochromism. *J. Chem. Phys.* **2002,** *116*, 8596.

(38) Heimel, G.; Daghofer, M.; Gierschner, J.; List, E. J. W.; Grimsdale, A. C.; Müllen, K.; Beljonne, D.; Brédas, J.-L.; Zojer, E. Breakdown of the mirror image symmetry in the optical absorption/emission spectra of oligo (para-phenylene) s. *J. Chem. Phys.* **2005,** *122*, 054501.

(39) Shi, J.; Aguilar Suarez, L. E.; Yoon, S.-J.; Varghese, S.; Serpa, C.; Park, S. Y.; Lüer, L.; Roca-Sanjuán, D.; Milián-Medina, B.; Gierschner, J. Solid state luminescence enhancement in π-conjugated materials: unraveling the mechanism beyond the framework of AIE/AIEE. *J. Phys. Chem. C* **2017,** *121*, 23166.

(40) The radiative rates k_F are supposed to be directly proportional to the oscillator strength f of the emitting state, as expressed by the Strickler-Berg equation, see e.g. Ref. 37. For Ph- and Th-TBN, TD-DFT gave very similar values for f (0.62, 0.83), while f of TBN is 0.28 (see Figure S15). The same trend is found for k_F (Table 1), i.e. 0.12, 0.27, 0.30 ns^{-1} for TBN, Ph-TBN and Th-TBN, respectively.

(41) Englman, R.; Jortner, J. The energy gap law for radiationless transitions in large molecules. *Mol. Phys.* **1970,** *18*, 145.

(42) Hoche, J.; Schulz, A.; Dietrich, L. M.; Humeniuk, A.; Stolte, M.; Schmidt, D.; Brixner, T.; Würthner, F.; Mitric, R. The origin of the solvent dependence of fluorescence quantum yields in dipolar merocyanine dyes. *Chem. Sci.* **2019,** *10*, 11013.

(43) Ikemoto, K.; Tokuhira, T.; Uetani, A.; Harabuchi, Y.; Sato, S.; Maeda, S.; Isobe, H. Fluorescence enhancement of aromatic macrocycles by lowering excited singlet state energies. *J. Org. Chem.* **2020,** *85*, 150.

(44) Izquierdo, M. A.; Shi, J.; Oh, S.; Park, S. Y.; Milián-Medina, B.; Gierschner, J.; Roca-Sanjuán, D. Excited-state non-radiative decay in stilbenoid compounds: an ab initio quantum-chemistry study on size and substituent effects. *Phys. Chem. Chem. Phys.* **2019,** *21*, 22429.

(45) Lanzani, G.; Nisoli, M.; Silvestri, S. D.; Tubino, R. Structural relaxation of photoexcited quaterthiophenes probed with vibrational specificity. *Chem. Phys. Lett.* **1996,** *251*, 339.

(46) Crespo-Otero, R.; Li, Q.; Blancafort, L. Exploring potential energy surfaces for aggregation-induced emission—from solution to crystal. *Chem. Asian J.* **2019,** *14*, 700.

(47) Gierschner, J.; Shi, J.; Milián-Medina, B.; Roca-Sanjuán, D.; Varghese, S.; Park, S. Luminescence in crystalline organic materials: from molecules to molecular solids. *Adv. Opt. Mater.* **2021,** *9*, 2002251.

Table of Contents